GSICS Inter-Calibration of Infrared Channels of Geostationary Imagers Using Metop/IASI

Tim J. Hewison, *Senior Member, IEEE*, Xiangqian Wu, Fangfang Yu, Yoshihiko Tahara, Xiuqing Hu, Dohyeong Kim, and Marianne Koenig

***Abstract*—The first products of the Global Space-based Inter-Calibration System (GSICS) include bias monitoring and calibration corrections for the thermal infrared (IR) channels of current meteorological sensors on geostationary satellites. These use the hyperspectral Infrared Atmospheric Sounding Interferometer (IASI) on the low Earth orbit (LEO) Metop satellite as a common cross-calibration reference. This paper describes the algorithm, which uses a weighted linear regression, to compare collocated radiances observed from each pair of geostationary-LEO instruments. The regression coefficients define the *GSICS Correction*, and their uncertainties provide quality indicators, ensuring traceability to the selected community reference, IASI. Examples are given for the Meteosat, GOES, MTSAT, Fengyun-2, and COMS imagers. Some channels of these instruments show biases that vary with time due to variations in the thermal environment, stray light, and optical contamination. These results demonstrate how inter-calibration can be a powerful tool to monitor and correct biases, and help diagnose their root causes.**

***Index Terms*—Calibration, earth observing system, infrared image sensors, international collaboration, meteorology, satellites.**

I. Introduction

THE GLOBAL Space-based Inter-Calibration System (GSICS) is an international collaborative effort which aims at ensuring consistent accuracy among space-based observations worldwide for climate monitoring, weather forecasting, and environmental applications [1]. This is achieved through a comprehensive calibration strategy, which involves monitoring instrument performances, operational inter-calibration of satellite instruments, tying the measurements to absolute references and standards, and recalibration of archived data. A major part of this strategy involves direct comparison of collocated observations from pairs of satellite instruments, which are used to systematically generate calibration functions to compare and correct the biases of *monitored instruments* to references. These *GSICS Corrections* are needed for accurately integrating data from multiple observing systems into, both near-real-time and re-analysis, products, applications, and services.

One of the first objectives of GSICS was to develop inter-calibration products for the infrared (IR) channels of geostationary (GEO) imagers as they are operated by several member organizations, including CMA, EUMETSAT, JMA, KMA, ISRO, and NOAA, and because the IR Atmospheric Sounding Interferometer (IASI) can provide high quality hyperspectral reference observations from its low Earth orbit (LEO) *Metop* platform [2]. This inter-calibration is based on the comparison of collocated GEO-LEO observations, as illustrated schematically in Fig. 1. It has been shown that IASI can be used as an excellent inter-calibration reference because it has been well characterized pre-launch, and its calibration has proven to be stable in-orbit and consistent with the Advanced IR Sounder (AIRS), which operates on the Aqua satellite, with standard uncertainties $\sim$0.1 K $(k = 1)$ [3], [4].

GSICS originally developed an inter-calibration algorithm for GEO-LEO IR using Aqua/AIRS as a reference [5]. However, as IASI has proved suitable and provides more continuous spectral coverage, it has now been adapted as the community reference for GEO-LEO IR inter-calibration products.

Like Metop, Aqua is a sun-synchronous LEO platform, but provides coverage around 1:30 satellite local time (SLT) to

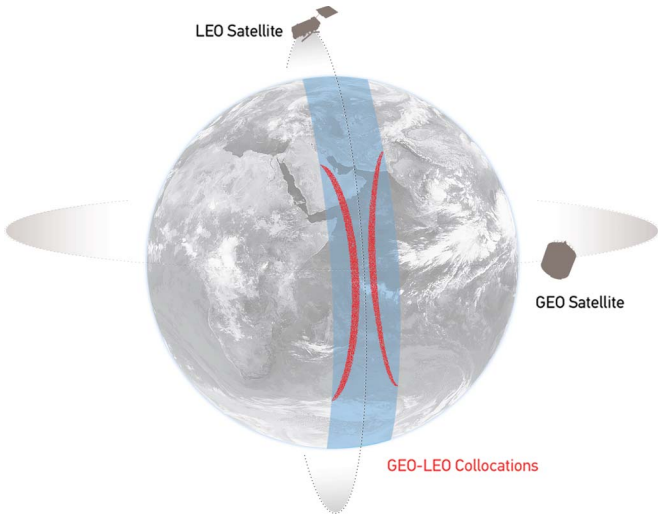

Fig. 1. Schematic illustration of the geostationary orbit (GEO) and polar low Earth orbit (LEO) satellites and distribution of their collocated observations.

Manuscript received February 21, 2012; revised July 25, 2012; accepted September 1, 2012. Date of publication February 5, 2013; date of current version February 21, 2013.

T. J. Hewison and M. Koenig are with EUMETSAT, Darmstadt 64295, Germany (e-mail: tim.hewison@eumetsat.int; marianne.koenig@eumetsat.int).

X. Wu is with NOAA/NESDIS/STAR, College Park, MD 20740 USA (e-mail: xiangqian.wu@noaa.gov).

F. Yu is with the Earth Resources Technology, Inc, Laurel, MD 20707 USA (e-mail: fangfang.yu@noaa.gov).

Y. Tahara is with the System Engineering Division, Meteorological Satellite Center, Japan Meteorological Agency, Tokyo 204-0012, Japan (e-mail: y-tahara@met.kishou.go.jp).

X. Hu is with NSMC/CMA, Beijing 100081, China (e-mail: huxq@cma.gov.cn).

D. Kim is with the National Meteorological Satellite Center, Korea Meteorological Administration, Seoul 156-720, Korea (e-mail: dkim@kma.go.kr).

Color versions of one or more of the figures in this paper are available online at http://ieeexplore.ieee.org.

Digital Object Identifier 10.1109/TGRS.2013.2238544

complement Metop's coverage around 9:30 SLT. The GSICS inter-calibration products described here are being extended to include the use of Aqua/AIRS as a calibration *transfer reference*, allowing better representation of the GEO imagers' diurnal variations, following the concept described in [6].

Although there are differences between the GEO imagers, their inter-calibration can be based on common principles. Observations from the *monitored* and *reference instruments* are collocated, transformed, compared, and analyzed to produce calibration correction functions, *GSICS Corrections*, which transform the observations' calibration to be consistent with a common reference.

The GSICS corrections described here are derived from a development of algorithms previously presented for the inter-calibration of GEO-LEO IR channels using hyperspectral reference instruments [5]–[8]. These represent a significant advance on previous work using reference instruments with broad-band channels [9]–[13], because of the increased ability to accurately represent the spectral response functions (SRFs) of the GEO imagers.

Although it is possible to develop independent inter-calibration products specially tuned for specific instruments, one of the aims of GSICS is to ensure consistency between different instruments. Hence, we have selected a basic algorithm for the inter-calibration of all instruments in the GEO-LEO IR class, based on common principles described below. Details of the algorithm are specified in a hierarchical approach, allowing fine-tuning for each particular implementation if necessary. This ensures the maximum consistency and traceability is achieved, while preserving the flexibility to tailor each inter-calibration optimal for the pair of instruments in question.

II. Inter-Calibration Algorithm

A. Principles

The basic premise of inter-calibration is that two instruments should make identical measurements when they view the same target at the same time, with the same spatial and spectral responses, and the same viewing geometry. Since these idealized conditions never occur in reality, a series of thresholds are applied to collocate the data, which is then transformed to a comparable scale.

GSICS has three broad objectives. The first objective is to quantify the bias, or the difference between a monitored and reference instrument, for the collocated data. This is useful because the results are generalized, albeit often implicitly, to measurements by the same pair of satellites not being directly compared. The second objective is to correct for the bias. Again, the efficacy of correction can only be validated with the collocated data but is assumed to hold for all measurements. The third objective is to find the causes of biases, thus to eliminate them from the root.

It may be that an apparent bias in the radiometric calibration can be introduced by an error in another component of the system—such as the SRF. Although ultimately the term in error should be corrected, it is also possible to compensate for its effect by applying a correction to the calibrated radiance, if the biases are sufficiently small to be linear.

For all these objectives, it is important to evaluate the bias, correction, and cause analysis collectively, or separately, under a variety of conditions. This dictates that the collocated measurements should adequately cover the normal range of several aspects of data acquisition. First, the collocations should cover all spectral bands, which enables users to quantify possible spectral variation of bias.

Second, the collocations should cover all scene radiances, which enables users to quantify possible scene dependence of bias. For this reason, it is desirable to reduce the size of collocation, to single pixels, if possible. Collocations over large areas have other advantages, for example they are less sensitive to target non-uniformity and temporal non-concurrence; however, they tend to smooth out scene temperature variability.

Next, the collocations should, in principle, cover all ranges of geographic location, viewing geometry, and time of day, which enables users to quantify possible geographic, geometric (angular), and diurnal variation of bias. These all require that the collocations include those away from the GEO nadir. Note that both AIRS and IASI are on a sun-synchronous orbit (Aqua and Metop, respectively), which means they always pass the nadir of a GEO satellite at the fixed local time of day.

Finally, the collocations should cover all days of year and all stages of satellite age, to enable users to quantify possible seasonal variation and long-term trend of bias. This requires that GSICS be operated continuously throughout the life time of satellites.

In summary, GSICS objectives require that single pixel collocations anywhere within the GEO field of regard (FOR) be collected continuously over long term for all bands.

As mentioned before, few collocations will be perfect; they are considered "collocated" if within certain thresholds. Another principle for the GSICS algorithm is to include observations from all sky conditions and to set the threshold values reasonably tight to keep the data volume manageable, meanwhile sufficiently tolerant to generate robust statistics, while allowing us to further investigate whether the calibration depends on several variables, such as radiance and incidence angle.

Throughout the inter-calibration process, it is important to propagate the uncertainty introduced at each stage. It is only in this way that we can ensure full traceability to a common reference. A detailed uncertainty analysis for the inter-calibration of Meteosat/Spinning Enhanced Visible and IR Imager (SEVIRI) using Metop/IASI as a reference is presented in a partner paper [14]. Ultimately, it is highly desirable to use an inter-calibration reference which is traceable to an internationally accepted standard such as the International System of Units (SI). While this is not yet the case for AIRS or IASI and is beyond the scope of this paper, it is noted that the GSICS framework will facilitate such traceability once a suitable standard becomes available in orbit, such as the Climate Absolute Radiance and Refractivity Observatory [15] mission.

B. Overview of the Inter-Calibration Algorithm

Fig. 2 provides an overview of the steps involved in the inter-calibration algorithm and acts as a map for this paper.

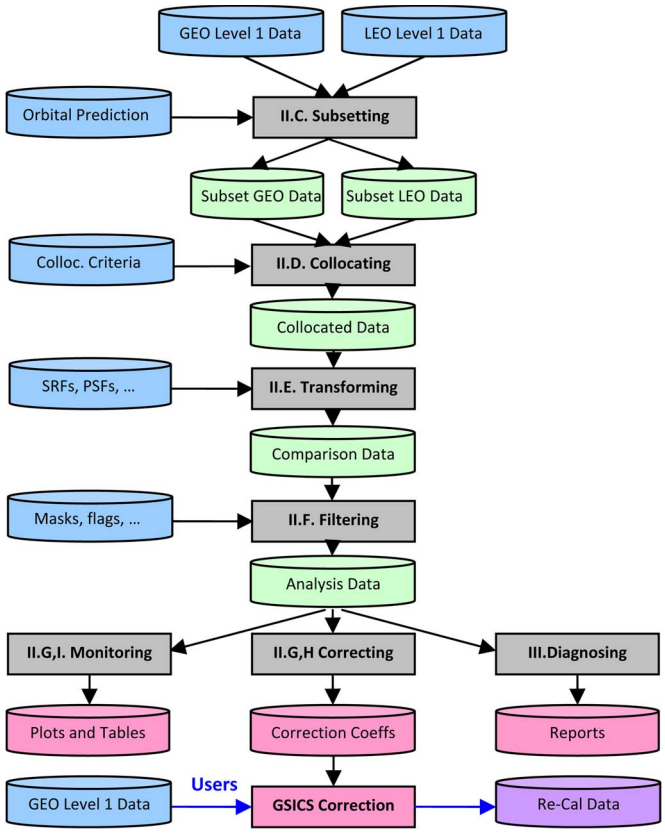

Fig. 2. Flowchart of overview of GSICS algorithm for the inter-calibration of infrared channels of a geostationary satellite instrument (GEO) using a reference instrument on a low Earth orbit (LEO) satellite. Gray boxes show processes and refer to the section numbering of this paper. Blue/pink shaded drums show input/output data sets, respectively. Users can apply the generated coefficients in a *GSICS Correction* to re-calibrate level 1 GEO radiances.

C. Subset Data

Only a minority of LEO observations are within a GEO's FOR, and only a small portion of these are concurrent with those of the GEO sensor. Also, a LEO granule collocated with a GEO image in time and space covers only a small portion of the GEO image. As a result, only a small subset of both GEO and LEO data, typically 2–5%, can generate collocations. It helps to identify this small subset of data to greatly improve the efficiency of the algorithm.

The GEO FOR is defined in this context as any locations whose arc angle (angular distance) to GEO nadir is less than a threshold of 53°. This gives a maximum GEO zenith angle similar to that of the LEO reference instrument, IASI ($\sim 60°$).

Although it is desirable, in principle, to represent the full diurnal cycle with collocations, there are particular limitations in the GEO-LEO IR case, which have made it necessary to restrict the comparisons to night-time only when generating GSICS Corrections. This helps avoid the impacts of possible directional reflectance/emissivity in the day-time window-channel IR data [16] and midnight calibration problems experienced by three-axis stabilized satellites (described later). Because of this limitation, clear guidance should be provided to users in the application of the GSICS Corrections to other periods of the diurnal cycle.

For the portions of each LEO orbit found to be within the monitored GEO's FOR, the equator crossing time is identified, and the GEO image sampled nearest to this time is selected, but only if it is within half of the GEO's refresh rate.

D. Find Collocations

The next step is to identify the pixels that are spatially collocated, temporally concurrent, geometrically aligned, and spectrally compatible.

1) Collocation in Space: We first extract the central location of each instruments' pixels and determine which pixels can be considered to be collocated, based on their centers being separated by less than a pre-determined threshold distance. For the GEO-LEO IR case, this threshold is defined as the radius of the LEO field of view (FoV) at nadir, which is 6 km for IASI.

2) Concurrent in Time: Those pixels identified as being spatially collocated are then tested to check whether the observations from both instruments were sampled sufficiently closely in time—i.e., separated by no more than a specific threshold of time difference. This threshold is chosen to allow a sufficient number of collocations, while not introducing excessive noise or bias due to the scenes' random or systematic variability in time. In the GEO-LEO case, this threshold is usually defined at 300 s, as the variability of GEO radiances over this period has been found to be comparable to that on spatial scales of the corresponding collocation threshold [14]. The actual threshold used is specified to allow more collocations for instruments with slower refresh rates, as shown in Table I.

3) Alignment in Viewing Geometry: We also ensure the selected collocated pixels have been observed under comparable conditions. This means they should be aligned such that they view the surface at similar incidence angles through similar atmospheric paths. Although in general this includes azimuth

TABLE I
TYPICAL REFRESH RATE AND CONCURRENCY THRESHOLD FOR CURRENT GEOSTATIONARY IMAGERS

Platform /Sensor	Typical refresh rate (min)	Collocation time threshold (min)	FoV diameter at nadir (km)	# pixels /target area *nxm*
Metop/IASI	100	5	12	1x1
Aqua/AIRS	100	5	13.5	1x1
Meteosat/MVIRI	30	15	5	3x3
Meteosat/SEVIRI	15	5	3	5x5
GOES Imager	15	5	4	5x3
MTSAT-2	30	5	4	3x3
COMS	30	5	4	3x3
FY-2 Imager	30/60	15	5	3x3

and polarization, only the elevation angles are considered in the GEO-LEO IR case.

Each candidate pixel is tested to check whether the viewing geometry of the observations from both instruments was sufficiently close. The criterion for zenith angle is defined according to the difference in the secant of the observations' zenith angles. Only pixels for which this is less than a predetermined threshold are included in further analysis. For the GEO-LEO IR case, this threshold is usually defined as 0.01, corresponding to a maximum 1% difference in atmospheric path length. This results in collocations being distributed approximately symmetrically about the equator mapping out a characteristic "slanted hourglass" pattern, as shown in Fig. 1.

E. Transform Data

In this step, collocated data are transformed to allow their direct comparison. These transformations can include modifying the spectral, temporal and spatial characteristics of the observations and require accurate knowledge of the instruments' characteristics. The outputs of this step are the best estimates of the channel radiances, together with estimates of their uncertainty.

1) Spectral Transformation: In general, we first need to identify which channel sets provide sufficient common information to allow meaningful inter-calibration by considering their nominal SRFs. These are then transformed into comparable *pseudo channels*, accounting for the deficiencies in channel matches. The observations of channels identified as comparable are then co-averaged using pre-determined weights to give pseudo channel radiances. A radiative transfer model (RTM) can be used to account for any differences in the pseudo channels' characteristics and estimate the uncertainty due to spectral mismatches.

This process is greatly simplified for most IR channels of GEO imagers when using a hyperspectral reference instrument, such as IASI, because its observed LEO radiance spectra, $L_{LEO}(\nu)$, can simply be convolved with the GEO instrument's SRFs, $\Phi(\nu)$, as $L_{GEO|LEO}$

$$L_{GEO|LEO} = \frac{\int\limits_{\nu} L_{LEO}(\nu)\Phi_{GEO}(\nu)d\nu}{\int\limits_{\nu} \Phi_{GEO}(\nu)d\nu}. \quad (1)$$

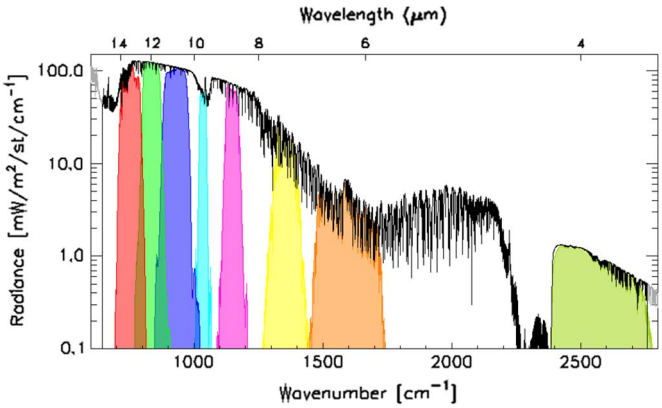

Fig. 3. Example radiance spectra measured by IASI (black) and modeled by LBLRTM (gray), convolved with the Spectral Response Functions of SEVIRI channels 3–11 from right to left (colored shaded areas). n.b. The IASI observations (645–2760 cm^{-1}) do not quite cover the full spectrum observed by SEVIRI.

However, this is not always the case. For example, the SRF of the 3.9 μm channel of Meteosat-9/SEVIRI extends beyond the short-wave limit of IASI, as shown in Fig. 3—or when using AIRS as a reference instrument, which does not provide continuous spectral coverage and has several bad channels. In these cases, the observed radiance spectra can be augmented by defining *virtual channels*, based on regression with synthetic spectra generated by RTMs. The *constrained optimization* method [17] is recommended, which estimates radiances over the missing spectral coverage, $L_{LEO}^{\mathrm{missing}}$, by a linear combination of simulated radiances $L_{LEO,k}^{\mathrm{simulate}}$

$$\ln L_{LEO}^{\mathrm{missing}} = c_0 + \sum_k c_k \ln L_{LEO,k}^{\mathrm{simulate}}. \quad (2)$$

$L_{LEO,k}^{\mathrm{simulate}}$ are generated in advance by using the line-by-line code (LBLRTM, [18]), with the HITRAN2004 spectroscopy line parameter database [19] including the AER updates version 2.0 [20] with respect to atmospheric model profiles k including clear and cloudy weather conditions over the tropics and mid latitudes, where GEO-LEO collocations occur. The coefficients c_k, which represent weights of the summation, are computed by regression analysis using validly observed LEO radiances for each GEO IR channel and each LEO pixel.

This spectral band adjustment procedure adds a small uncertainty to the short-wave channels when using IASI as a reference, which is evaluated in [14]. However, it is likely to dominate the uncertainty when using AIRS as a transfer reference, which is currently undergoing full evaluation.

2) Spatial Matching: We identify the pixels that define the *target area* around each collocation. For the GEO-LEO case the target area is defined by rectangular grids of $n \times m$ GEO pixels, where n and m are chosen to correspond to area which encloses the collocated LEO FoV, with a minimum of 9 'independent' pixels. This ensures it covers all the contributing radiation in event of small navigation errors, while being large enough to ensure reliable statistics of the variance are available. An example of the target area is shown in Fig. 4.

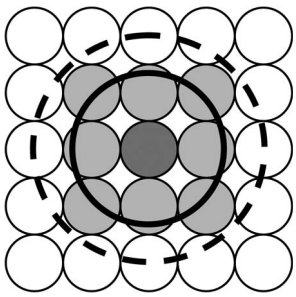

Fig. 4. Illustration of spatial transformation. Small circles represent the GEO FoVs, and the two large circles represent the LEO FoV for the extreme cases of FY2-IASI, where $n \times m = 3 \times 3$ and SEVIRI-IASI, where $n \times m = 5 \times 5$. (Adapted from [5]).

The radiances measured in the GEO pixels within the target area are then averaged and their variance calculated to estimate the uncertainty on the average due to spatial variability, accounting for any oversampling.

Several caveats should be noted of the idealized illustration of Fig. 4. All FoVs in Fig. 4 are circular in shape, with no undersampling or oversampling between the adjacent FoVs. These are typical, but not always true. Moreover, regardless of the shape, in general, the transformed GEO radiance covers a little more or less than the LEO FoV, never exactly 100%. The dark-shaded GEO FoV in the center represents the one that is closest to the center of LEO FoV. The two centers are perfectly aligned in Fig. 4, which is not generally the case in reality. The effects of spatial response of both instruments, such as point spread function, are ignored. Finally, the relative position of GEO and LEO FoVs are based on operational geolocation of respective instruments, which have their own errors, the impact of which is assessed as negligible in [14]. Together, these caveats mean that the transformed GEO radiance is an approximation of the radiance from LEO FoV that is measured by GEO.

F. Filter Collocations

To prevent anomalous observations having undue influence on the results, outliers may be identified and rejected on a statistical basis. If a small number of anomalous pixels appear only in one sensor's FoV but not the other, it can cause unwanted bias in a single comparison. To check for spatial inhomogeneity, an extended area is defined around each target, referred to as the *environment*, defined to cover approximately twice the target area, as shown in Fig. 5. Radiances in the target area are compared with those in the surrounding *environment*, and those which are significantly different from the environment $(> 3\sigma)$ are rejected.

Although it is also possible to filter the collocations, by applying a threshold to the variance of the target area pixels' radiance, this approach was found to be sub-optimal compared to using this variance as part of a weighted regression, as this allows better representation of the full range of radiances—including partially cloudy scenes, which have intermittent radiance, but are highly variable.

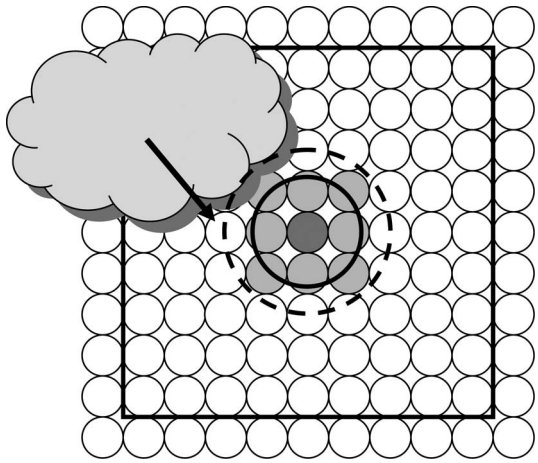

Fig. 5. As Fig. 3, but extended to show the *environment*, defined in this case as an array of 9×9 GEO pixels. Inhomogeneities within the environment which can influence the collocation can be filtered out. (Adapted from [5]).

G. Compare Collocations—Using Linear Regression

The basis of the comparison is the weighted linear regression of collocated radiances in pairs of channels and pseudo channels from the monitored and reference instruments. This is performed independently for each channel of the monitored instrument. The weights, w_i, are defined as the inverse of the sum of the spatial and temporal variance of the target radiance, s_x and s_t, and the radiometric noise, δ_{GEO}, squared

$$w_i = \frac{1}{s_x + s_t + \delta_{GEO}^2}. \tag{3}$$

Together these provide an estimated uncertainty on each dependent point, $w_i^{-1/2}$. In practice, the measured spatial variance, s_x, is used as a proxy for the temporal variance, s_t, as these are found to be comparable when using the above collocation criteria in a detailed uncertainty analysis [14]. Including the radiometric noise, δ_{GEO}, ensures that very homogeneous targets scenes where all the pixels give the same radiance do not have undue influence on the weighted regression. However, the contribution of the LEO radiometric noise is assumed to be negligible, as hundreds of IASI channels are averaged in the spectral transformation.

Fig. 6 shows an example of the linear regression calculated using collocation targets acquired on one night (2012-01-12) from Meteosat-9/SEVIRI and Metop-A/IASI. There is often more collocation data at higher radiances, corresponding to clear sky scenes, for which the results are optimized as applications in these conditions put the most demanding requirements on calibration accuracy. This may be reviewed in future, if greater emphasis is needed for low radiance scenes, corresponding to cold cloud tops.

H. Calculate Coefficients for GSICS Corrections

The regression produces estimates of coefficients describing the slope, b_r, and offset, a_r, of the relationship between the two instruments' radiances with their uncertainties, expressed as a covariance. Together, these make up the coefficients of the *GSICS Correction*, which can be applied by inverting the

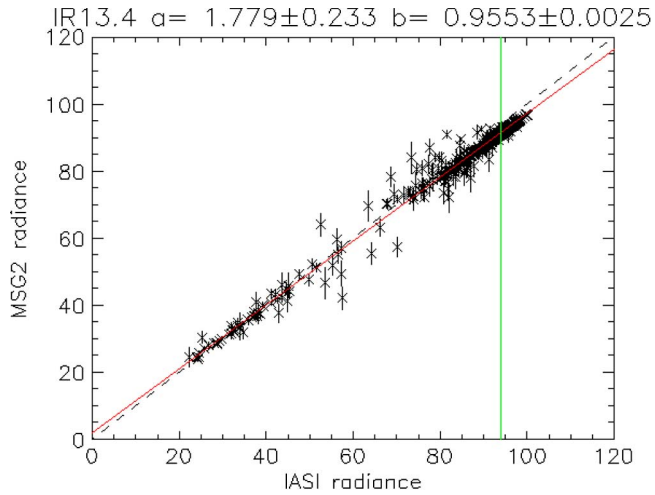

Fig. 6. Example of linear regression of collocated radiances from the 13.4 μm channel of Meteosat-9/SEVIRI ("MSG2") and Metop-A/IASI. Radiance units are mW/m^2/sr/cm^{-1}. Each point shows the mean radiance of one collocation target, with an error bar representing the weight used in the regression. Dashed line shows 1:1 relationship that would be followed if the instruments' calibration were consistent. Red solid line shows regression fit given by coefficients in the plot title. The vertical green line indicates the standard scene radiance at which the standard bias is evaluated, corresponding to the difference between the red and dotted lines at this point.

regression relationship to estimate a corrected radiance for a given GEO radiance, L_{GEO}

$$\hat{L}_{LEO} = -\frac{a_r}{b_r} + \frac{1}{b_r} L_{GEO}. \tag{4}$$

Collocations from a time series of inter-comparison results are combined to reduce the random component of the uncertainty on the final GSICS Correction. This requires the definition of a representative *smoothing period* over which the results can be smoothed without introducing bias due to calibration drifts. This period is defined by comparing the maximum observed rate of change of bias with a pre-determined threshold, based on the required or achievable accuracy. This results in a smoothing period of $\sim$1 month being used for the IR channels of current GEO imagers.

Sometimes, GEO instrument performance may indeed have short-term variation. An extreme example is the occasional instrument decontamination, which is known to change instrument performance. Another more common example is that GEO bias can vary diurnally, particularly those on three-axis stabilized platforms. For these reasons, only the similar data are used for regression, and periods, such as diurnal cycles and decontamination events, are analyzed separately.

Coefficients for *Re-Analysis Corrections* are calculated from the regression of all collocations symmetrically distributed within the smoothing period, centered on the reference date. For *Near-Real-Time Corrections*, only collocations sampled within this half this period, prior to the current date, are used in the regression. This allows the results to be more representative of the monitored instrument's performance on a given date, without being significantly biased by any trends. The results are monitored and any significant changes to the instrument's operation or performance trigger a *reset* of the smoothing period, which is flagged in the files containing the coefficients of the GSICS Corrections. This ensures unbiased results are obtainable immediately before and after events such as spacecraft decontaminations.

Although the coefficients' uncertainties provide useful quality indicators, they do not represent all the processes that can introduce errors into the inter-calibration, which have been analyzed in detail [14], which recommends scaling the quoted uncertainties by a factor to better represent the total uncertainty of the GSICS Correction.

I. Generate GSICS Bias Monitoring Plots

The routine comparisons of an instrument against the reference provide a useful tool for monitoring the performance of its radiometric calibration. The relative bias of the monitored instrument is evaluated using the regression coefficients and is plotted as time series, known as *GSICS Bias Monitoring*.

Because biases can be radiance dependent, it is necessary to define channel-specific *standard radiances*, at which instruments' inter-calibration bias can be directly compared and conveniently expressed in units readily understandable, such as brightness temperatures (Tb). The standard radiances are calculated using an RTM based on a standard atmospheric profile and surface conditions. For each IR channel, they are calculated accounting its SRF under the following conditions: at nadir, at night in a 1976 US Standard Atmosphere, in clear skies, over the sea with a surface temperature of $+15$ °C and a wind speed of 7 m/s using the RTTOV9.2 fast model [21]. Conversions between radiance and brightness temperatures are instrument specific, according to the operators' recommendations, which are given in the meta data of the GSICS Correction files.

III. Example Results

The GSICS Processing and Research Centers responsible for each satellite instrument publish routinely updated bias monitoring plots on their web pages, which are accessible through the GSICS portal: http://gsics.wmo.int. Example results for various GEO imagers are given here, with some discussion of the features shown to illustrate the concept of root cause analysis that can be conducted from these. These are all expressed in terms of *standard biases*—i.e., those derived by evaluating the GSICS Corrections for standard radiance scenes. In general, the resulting radiance biases vary with scene temperature—usually decreasing in cold scenes.

A. Meteosat/SEVIRI and MVIRI From EUMETSAT

Meteosat-8 and -9 are the first GEO satellites of EUMESAT's Meteosat Second Generation (MSG) program. Each carries a SEVIRI, which has eight IR channels between 3.9 μm and 13.4 μm, and can provide full disk images every 15 min with a 3 km sampling interval at nadir [22].

An example time series of the relative bias of each IR channel of Meteosat-9/SEVIRI is shown in Fig. 7. The standard uncertainties $(k = 1)$ on these biases are estimated to be $\sim$0.01 K [14]. Most IR channels of Meteosat-9 and all those of Meteosat-8

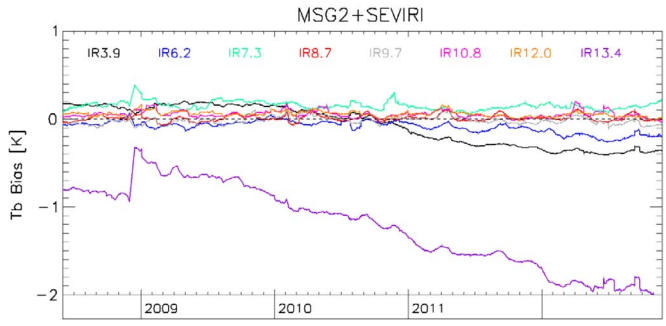

Fig. 7. Example time series plot showing relative bias of IR channels of Meteosat-9/SEVIRI (MSG2) wrt Metop-A/IASI, expressed as brightness temperature difference for standard radiance scenes (corresponding to a 1976 US Standard Atmosphere with clear sky). A spacecraft decontamination in Dec 2008 reduced the bias of the 13.4 μm channel.

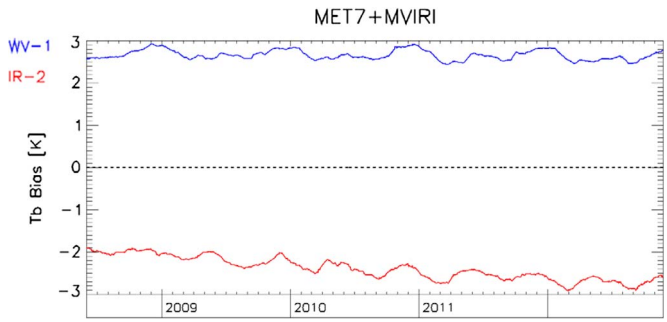

Fig. 8. As Fig. 7 for WV (blue) and IR (red) channels of Meteosat-7/MVIRI.

(not shown) had small (< 0.4 K) and stable biases during this period. However, the 13.4 μm channel of Meteosat-9 shows a negative bias, which slowly grows larger until a spacecraft decontamination event takes place in early December 2008. Thereafter, this channel continues its degradation, which is believed to be caused by an accumulation of ice on the surface of its optics, which modifies the SRF of this channel [23]. The bias of the 13.4 μm channel of Meteosat-9 does not return to zero even immediately after the decontamination, which suggests the residual error may be due to an inaccurate representation of the SRF, which is not the case for Meteosat-8.

Meteosat-7/MVIRI is the last of the first generation of GEO imagers operated by EUMETSAT. It was launched in 1997 and has been operating over the Indian Ocean since Nov 2006. Although it includes onboard black body calibration, its water vapor and IR channels have much larger mean biases than their SEVIRI counterparts during this period (+2.7 K for the WV channel, −2.3 K for the IR channel), as shown in Fig. 8, which show pronounced annual and semi-annual cycles. The IR channel also shows a gradual degradation, which may also be due to a build-up of contamination on the optics.

B. GOES From NOAA

GSICS corrections have been generated for the IR channels of operational GOES since after 2007. To avoid the GOES IR midnight calibration anomaly [24], only the night-time IASI collocation data before 22:30 SLT are used to generate the correction coefficients. The GOES Imager IR midnight calibration anomaly becomes apparent after 22:30 until around

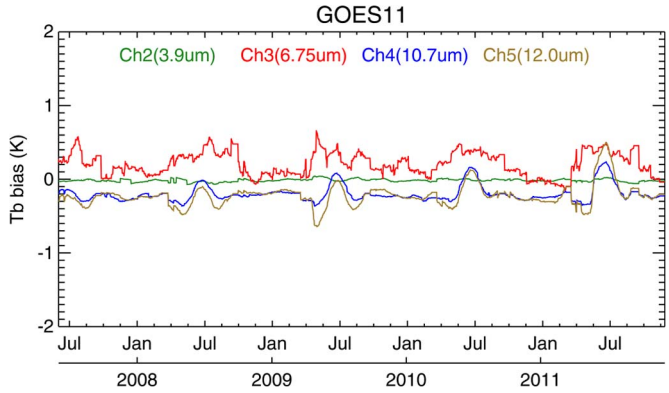

Fig. 9. As Fig. 7 for IR channels of GOES-11 Imager.

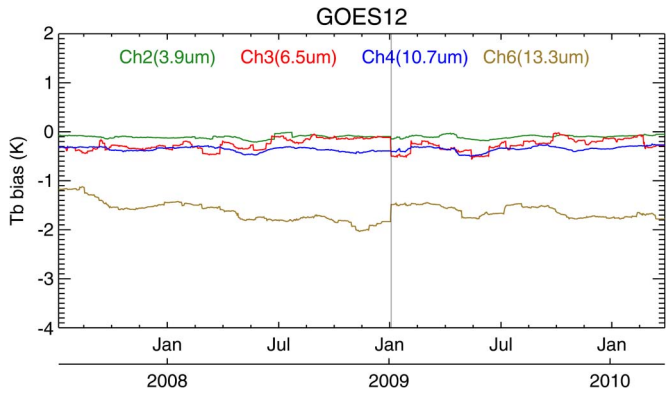

Fig. 10. As Fig. 7 for GOES-12 Imager IR channels. The impact of the anti-ice decontamination event in early Jan 2009 can be observed in Ch3 (6.5 μm) and Ch6 (13.3 μm).

04:00 SLT [25]. Although an operational empirical correction for erroneous midnight calibration coefficients is available for the Imager IR channels, the performance of the empirical correction varies with time and channels, resulting in relatively large variation of the Tb bias at some channels, particularly at the long-wave IR channels [25]. Consequently, the GOES correction coefficients generated from night-time collocations is most appropriate for the GOES radiance beyond the satellite midnight anomaly period (22:30–04:00 SLT), but with relatively large uncertainty within this window period.

Example time series of the bias in the GOES-11 and GOES-12 Imager IR channels with respect to the night-time collocated IASI data are shown in Figs. 9 and 10. As shown in Fig. 9, the Tb bias in GOES-11 Ch2 is very consistent, while there are some seasonal variations in the Tb bias in the other three channels of this instrument. The seasonal changes of the Tb bias at Ch3 were mainly associated with the patch temperature change [5]. Further investigation is needed to understand the root cause of the seasonal variations of Tb biases in GOES-11 Imager Ch4 and Ch5.

GOES-12 Imager has the first channel centered at 13.3 μm in the series of GOES satellites. While the Tb biases with respect to IASI were within 0.5 K at the other three IR channels, Ch6 has a large and varying Tb bias, which was attributed to the erroneous ground-measured SRF as well as the impact of the failure of Imager anti-ice heater [24], [26]. To reduce the rate of signal loss due to the ice contamination, four decontamination

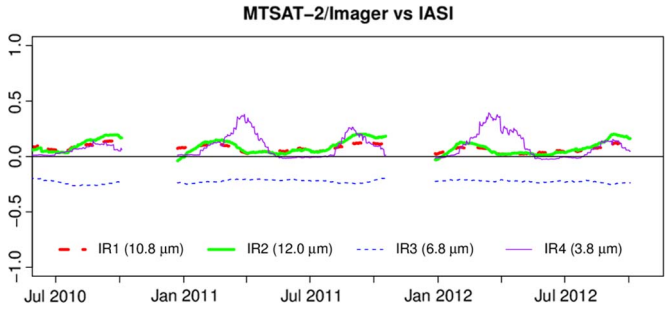

Fig. 11. As Fig. 7 for IR channels of MTSAT-2 Imager. MTSAT-2 operation was suspended in fall 2010 due to the ground system malfunction and maintenance and fall 2011 due to the maintenance.

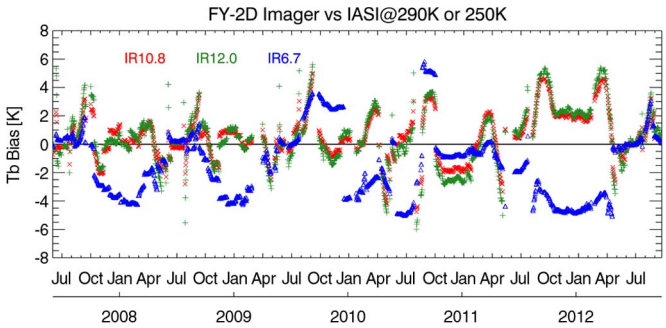

Fig. 12. As Fig. 7 for three long wave IR bands of FY-2-D Imager compared with IASI.

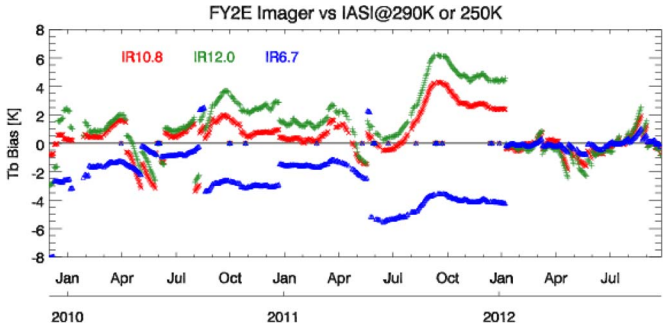

Fig. 13. As Fig. 7 for three long wave IR bands of FY-2E Imager compared with IASI.

events were conducted for GOES-12 Imager so far, including the ones in late Feb 2007, early July 2007, early Jan 2009, and late April 2010. As shown in Fig. 10, the impact of the decontamination event in early Jan 2009 can be observed at two absorptive channels, Ch3 (6.5 μm) and Ch6 (13.3 μm).

C. MTSAT From JMA

Multi-functional Transport Satellite 2 (MTSAT-2) carries an imager with four IR channels similar to GOES-11. Fig. 11 shows time series of the biases in the MTSAT-2 IR channels with respect to IASI from the beginning of its operation in June 2010. Except for the 3.8 μm channel, the biases are stable during this period, and the averages are +0.08 K for the 10.8 μm channel, +0.10 K for the 12 μm channel and −0.22 K for the 6.8 μm channel.

Since MTSAT-2 is a three-axis stabilized satellite, like GOES, a midnight effect on the calibration is also recognized, when the imager faces to the sun, and solar light degrades the MTSAT-2 calibration. The observed seasonal variations on the biases are similar to those reported for GOES [25].

D. Fengyun-2 From CMA

The Fengyun-2 (FY-2) series of GEO meteorological satellites carry imagers with four IR channels similar to GOES-11. Fig. 12 show time series of the biases in three long wave IR bands of FY-2-D with respect to IASI since May 2007. Most of the biases (@290 K) in split window bands are smaller than 2 K during non-autumn season (before and after September). The average biases are +0.40 K from IASI for the 10.8 μm band, +0.375 K for the 12 μm band, but there is a significant bias (up to 6 K) in the autumn eclipse season. Most of the biases (@250 K) in 6.7 μm water band are large (mean = −2.11 K wrt IASI) with clear seasonal dependence. The standard deviations of the biases of these three bands are all large (more than 1.5 K) over the past 5 years. This indicates that the stability of calibration of FY-2-D is not as good as other GEO satellites.

Fig. 13 shows time series of the biases in three long wave IR bands of FY-2E with respect to IASI since November, 2009. The average biases (@290 K) before 12 January 2012 are +0.31 K from IASI for the 10.8 μm band, +1.27 K for the 12 μm band. The biases (@250 K) in 6.7 μm water band is similarly large as FY-2-D (mean = −1.67 K). Although the biases of FY-2E are larger than FY-2-D, the seasonal fluctuation of the biases is smaller than FY-2-D because the standard deviations of the biases of these three bands are a little smaller than FY-2-D. The biases decrease dramatically to less than 0.2 K on 12 January 2012 when the operational calibration began to use inter-calibration similar to the GSICS algorithm described here. This indicates that GSICS correction lead to the significant improvement of the FY-2E calibration accuracy. The detailed calibration evaluation of FY-2 satellites can be seen in [27].

E. COMS From KMA

The Meteorological Imager on the Korean Communication, Ocean and Meteorological Satellite, COMS was launched in June 2010 and has a similar design to MTSAT-2 and GOES. Inter-calibration products are still under development, but example time series of the biases of its IR channels relative to IASI is shown in Fig. 14. These show the calibration of all channels was stable during 2011, but there were small negative biases around −0.2 K and −0.4 K in the 3.8 and 12.0 μm channels, respectively, and a small positive bias around +0.3 K and +0.4 K in the 6.8 and 10.8 μm channels, respectively. The causes of relatively large biases in the window channels are still under investigation.

IV. Conclusion

A common algorithm has been developed by the GSICS for the inter-calibration of the IR channels of current GEO imagers,

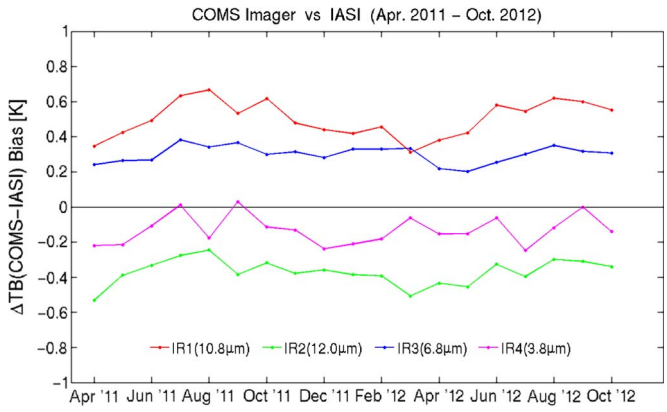

Fig. 14. As Fig. 7 for IR channels of COMS Meteorological Imager.

based on the direct comparison of collocated observations with Metop/IASI as a reference instrument. This is used to generate coefficients for *GSICS Corrections*, which users can apply to Level 1 radiances for both near-real-time and re-analysis applications.

The coefficients of the GSICS Corrections are published in netCDF format on dedicated servers, which are accessible through the GSICS portal: http://gsics.wmo.int. This also includes links to the instrument operators' web pages, where *GSICS Bias Monitoring* plots are regularly updated. These allow users to visualize time series of the biases that have been derived for each GEO imager from their inter-calibration for scenes corresponding to typical clear sky conditions. Although the biases are expressed in terms of brightness temperatures, the GSICS Corrections are based on radiances. Furthermore, the biases are radiance dependent. In most channels for low radiance scenes, corresponding to cold cloud tops, the linear regression coefficients of the GSICS Corrections are such that the radiance biases tend to be smaller (although they may appear to be larger when expressed in brightness temperature due to the nonlinearity of the Planck function). However, in cases where an incorrect SRF is assumed, the linear regression coefficients can produce erroneous bias for low radiance scenes and a quadratic function is needed to better correct the observed bias patterns [25], [28].

The example time series plots given in this paper show some channels of these instruments exhibit biases that vary with time due to variations in the thermal environment, stray light and optical contamination.

The monitoring and correction of satellite instruments' calibration are the first two of GSICS aims. The third objective of GSICS is to diagnose the root cause of bias. There have already been several successful examples of this. For example, the diagnosis and correction of error in GOES-13 Imager 13.3 μm channel SRF [28], [29], the ice contamination of the corresponding channel of Meteosat/SEVIRI [23], and the characterization of GOES Imager midnight blackbody calibration anomaly [25], [30], which have been discussed elsewhere.

These inter-calibration results have been derived over the limited geographical domains over which GEO-LEO collocations are available (which are concentrated in the tropics). Until now it has been assumed that the calibration of the monitored GEO instruments does not depend significantly on any variable other than the scene radiance and date. Analysis of the results for the IR channels of current GEO imagers confirms this to be a good approximation. However, further analysis [25] has shown that some sensors on 3-axis stabilized platforms may be subject to diurnal calibration variations, which require extensions to the basic method described here. These are currently being developed within GISCS by including Aqua/AIRS as a calibration transfer reference to increase the coverage of the diurnal cycle. The causes of other biases are still under investigation.

In summary, these results demonstrate how inter-calibration can be a powerful tool to monitor and correct biases, and help diagnose their root causes.

ACKNOWLEDGMENT

The authors are grateful to the many other people who have contributed to the development of this algorithm, in particular the current and former members of GSICS Research Working Group, including D. Blumstein, C. Cao, S.-R. Chung, D. Doelling, M. Gunshor, P. Henry, K. Kato, D. Kim, J. Lafeuille, J. Liu, P. Minnis, A. Okuyama, J. Privette, B.-J. Sohn, D. Tobin, X. Xiong, P. Zhang, and Y. Zhang. The anonymous reviewers' comments and advice were also greatly appreciated in improving this paper.

REFERENCES

[1] M. Goldberg, G. Ohring, J. Butler, C. Cao, R. Datla, D. Doelling, V. Gaertner, T. Hewison, B. Iacovazzi, D. Kim, T. Kurino, J. Lafeuille, P. Minnis, D. Renaut, J. Schmetz, D. Tobin, L. Wang, F. Weng, X. Wu, F. Yu, P. Zhang, and T. Zhu, "The global space-based inter-calibration system (GSICS)," *Bull. Amer. Meteorol. Soc.*, vol. 92, no. 4, pp. 468–475, Apr. 2011.

[2] D. Blumstein, B. Tournier, F. R. Cayla, T. Phulpin, R. Fjortoft, C. Buil, and G. Ponce, "In-flight performance of the infrared atmospheric sounding interferometer (IASI) on Metop-A," in *Proc. SPIE*, 2007, vol. 6684, pp. 66840H-1–66840H-12.

[3] L. Wang, M. Goldberg, X. Wu, C. Cao, R. A. Iacovazzi, Jr., F. Yu, and Y. Li, "Consistency assessment of AIRS and IASI radiances: Double differences versus simultaneous nadir overpasses," *J. Geophys. Res.*, vol. 116, no. D11, pp. D11111-1–D11111-11, Jun. 2011.

[4] GSICS traceability statement for IASI and AIRS, EUMETSAT, Darmstadt, Germany, EUMETSAT Tech. Note EUM/MET/TEN/11/0157. [Online]. Available: http://www.eumetsat.int/groups/sir/documents/document/pdf_trace_stat_iasi_airs.pdf

[5] X. Wu, T. Hewison, and Y. Tahara, "GSICS GEO-LEO inter-calibration: Baseline algorithm and early results," in *Proc. SPIE*, 2009, vol. 7456, pp. 745604-1–745604-12.

[6] G. Chander, T. J. Hewison, N. Fox, X. Wu, X. Xiong, and W. Blackwell, "Overview of inter-calibration of satellite instruments," *IEEE Trans. Geosci. Remote Sens.*, vol. 51, no. 3, pp. 1056–1080, Mar. 2013.

[7] L. Wang, C. Cao, and M. Goldberg, "Inter-calibration of GOES-11 and GOES-12 water vapor channels with MetOp/IASI hyperspectral measurements," *J. Atmos. Ocean. Technol.*, vol. 26, no. 9, pp. 1843–1855, 2009.

[8] M. M. Gunshor, T. J. Schmit, W. P. Menzel, and D. C. Tobin, "Intercalibration of broadband geostationary imagers using AIRS," *J. Atmos. Ocean. Technol.*, vol. 26, no. 4, pp. 746–758, Apr. 2009.

[9] W. P. Menzel, W. L. Smith, and L. D. Herman, "Visible infrared spin-scan radiometer atmospheric sounder radiometric calibration: An inflight evaluation from intercomparisons with HIRS and radiosonde measurements," *Appl. Opt.*, vol. 20, no. 20, pp. 3641–3644, Oct. 1981.

[10] F.-M. Brèon, D. L. Jackson, and J. J. Bates, "Calibration of the Meteosat water vapor channel using collocated NOAA/HIRS 12

measurements," *J. Geophys. Res.*, vol. 105, no. D9, pp. 11925–11933, Jan. 2000.
[11] S. A. Tjemkes, M. König, H.-J. Lutz, L. van de Berg, and J. Schmetz, "Calibration of Meteosat water vapor channel observations with independent satellite observations," *J. Geophys. Res.*, vol. 106, no. D6, pp. 5199–5209, Jan. 2001.
[12] M. M. Gunshor, T. J. Schmit, and W. P. Menzel, "Intercalibration of the infrared window and water vapor Channels on operational geostationary environmental satellites using a single polar-orbiting satellite," *J. Atmos. Ocean. Technol.*, vol. 21, no. 1, pp. 61–68, Jan. 2004.
[13] Z. Rong, Y. Zhang, F. Lu, J. Xu, and K. Qiu, "Inter-calibration of FY-2B IR channel with NOAA satellites," *Acta Meteorol. Sin.*, vol. 63, pp. 485–492, 2005.
[14] T. J. Hewison, "An evaluation of the uncertainty of the GSICS SEVIRI-IASI inter-calibration products," *IEEE Trans. Geosci. Remote Sens.*, vol. 51, no. 3, pp. 1171–1181, Mar. 2013.
[15] D. Anderson, K. W. Jucks, and D. F. Young, "The NRC decadal survey climate absolute radiance and refractivity observatory: NASA implementation," in *Proc. IEEE IGARSS*, Jul. 7–11, 2008, vol. 3, pp. III-9–III-11.
[16] P. Minnis, A. V. Gambheer, and D. R. Doelling, "Azimuthal anisotropy of longwave and infrared window radiances from CERES TRMM and Terra data," *J. Geophys. Res.*, vol. 109, no. D8, p. D08202, 2004.
[17] Y. Tahara and K. Kato, "New spectral compensation method for intercalibration using high spectral resolution sounder," *JMA Meteorol. Satell. Center Tech. Note*, no. 52, pp. 1–37, Feb. 2009.
[18] S. A. Clough and M. J. Iacono, "Line-by-line calculations of atmospheric fluxes and cooling rates II: Application to carbon dioxide, ozone, methane, nitrous oxide, and the halocarbons," *J. Geophys. Res.*, vol. 100, no. D8, pp. 16519–16535, Jan. 1995.
[19] L. S. Rothman, A. Barbe, D. Chris Benner, L. R. Brown, C. Camy-Peyret, M. R. Carleer, K. Chance, C. Clerbaux, V. Dana, V. M. Devi, A. Fayt, J.-M. Flaud, R. R. Gamache, A. Goldman, D. Jacquemart, K. W. Jucks, W. J. Lafferty, J.-Y. Mandin, S. T. Massie, V. Nemtchinov, D. A. Newnham, A. Perrin, C. P. Rinsland, J. Schroeder, K. M. Smith, M. A. H. Smith, K. Tang, R. A. Toth, J. Vander Auwera, P. Varanasi, and K. Yoshino, "The HITRAN molecular spectroscopic database: Edition of 2000 including updates through 2001," *J. Quant. Spectr. Radiat. Transf.*, vol. 82, no. 1–4, pp. 5–44, 15 Nov.–15 Dec. 2003.
[20] AER's Radiative Transfer Working Group, AER, Lexington, MA. [Online]. Available: http://rtweb.aer.com/main.html
[21] R. Saunders, M. Matricardi, and P. Brunel, "An improved fast radiative transfer model for assimilation of satellite radiance observations," *Q. J. R. Meteorol. Soc.*, vol. 125, no. 556, pp. 1407–1426, Apr. 1999.
[22] J. Schmetz, P. Pili, S. Tjemkes, D. Just, J. Kerkmann, S. Rota, and A. Ratier, "An introduction to Meteosat Second Generation (MSG)," *Bull. Amer. Meteorol. Soc.*, vol. 83, no. 7, pp. 977–992, Jul. 2002.
[23] T. Hewison and J. Mueller, "Ice contamination of Meteosat/SEVIRI implied by inter-calibration against Metop/IASI," *IEEE Trans. Geosci. Remote Sens.*, vol. 51, no. 3, pp. 1182–1186, Mar. 2013.
[24] R. X. Johnson and M. Weinreb, "GOES-8 imager midnight effects and slope correction," in *Proc. SPIE*, 1996, vol. 2812, pp. 596–607.
[25] F. Yu, X. Wu, M. K. R. V. Raja, Y. Li, L. Wang, and M. Goldberg, "Evaluations of diurnal calibration variation and scan angle emissivity calibration for GOES imager infrared channels," *IEEE Trans. Geosci. Remote Sens.*, vol. 51, no. 1, pp. 671–683, Jan 2013.
[26] F. Yu and X. Wu, "Correction for GOES imager spectral response function using GSICS II: Applications," *IEEE Trans. Geosci. Remote Sens.*, vol. 51, no. 3, pp. 1200–1214, Mar. 2013.
[27] X. Hu, N. Xu, F. Weng, Y. Zhang, L. Chen, and P. Zhang, "Long term monitoring and correction of IR calibration for FY-2 satellite imagers using AIRS and IASI," *IEEE Trans. Geosci. Remote Sens.*, to be published.
[28] X. Wu and F. Yu, "Correction for GOES imager spectral response function using GSICS. Part I: Theory," *IEEE Trans. Geosci. Remote Sens.*, vol. 51, no. 3, pp. 1215–1223, Mar. 2013.
[29] X. Wu, T. Schmit, R. Galvin, M. Gunshor, T. Hewison, M. König, Y. Tahara, D. Blumstein, Y. Li, S. Sohn, and M. Goldberg, "Investigation of GOES imager 13.3 μm channel cold bias," in *Proc. EUMETSAT Meteorol. Satell. Conf.*, Darmstadt, Germany, Sep. 8–12, 2008. [Online]. Available: http://www.eumetsat.int/Home/Main/AboutEUMETSAT/Publications/ConferenceandWorkshopProceedings/2008/SP_1232700911980?l=en
[30] M. K. Rama Varma Raja, X. Wu, and F. Yu, "Assessment of midnight blackbody calibration correction (MBCC) using the global space-based inter-calibration system (GSICS)," in *Proc. SPIE*, 2009, vol. 7456, p. 745603-1.

Tim J. Hewison (M'96–SM'13) received the Ph.D. doctorate in meteorology from the University of Reading, Berkshire, U.K., in 2006, based on his thesis on the use of ground-based microwave radiometers for atmospheric temperature and humidity profiling.

Currently, he is a Meteorological Scientist at EUMETSAT, Darmstadt, Germany, concentrating on the calibration of current, past, and future satellite instruments. He also currently chairs the Research Working Group of the Global Space-based Inter-Calibration System.

Xiangqian (Fred) Wu received the B.S. degree in geography from Beijing Normal University, Beijing, China, in 1982 and the Ph.D. degree in meteorology from the University of Wisconsin-Madison in 1990.

He joined NOAA/NESDIS/STAR, College Park, MD, as a Physical Scientist in 2002. Before that, he was an Associate Researcher, Assistant Scientist, and Associate Scientist at the Cooperative Institute for Meteorological Satellite Studies, University of Wisconsin-Madison from 1993 to 2002. Currently, he is the GOES and NPP/JPSS OMPS Instrument Scientist and the Co-chair of the Global Space-based Inter-Calibration System Research Working Group.

Fangfang Yu received the B.S. degree in geology and the M.S. degree in remote sensing and geographic information system from Beijing University, Beijing, China in 1991 and 1994, respectively, and the Ph.D. degree in geography from the University of Kansas, Lawrence, in 2002.

She is a Senior Research Scientist with Earth Resources Technology, Inc, Laurel, MD, in support of satellite sensor calibration for NOAA/NESDIS. Currently, she is the Deputy Director of the Global Space-based Inter-Calibration System (GSICS) Coordination Center, the Deputy Director of NOAA GSICS Processing and Research Center, and the Deputy for the GOES instrument calibration.

Yoshihiko Tahara received the Master of Engineering in physical electronics from Tokyo Institute of Technology, Tokyo, Japan, in 1992 based on his thesis on layout design of integrated circuits.

Currently, he is the Head of the system engineering division of the Meteorological Satellite Center, the Japan Meteorological Agency, Tokyo, engaging in the operation of the Japanese geostationary satellites, MTSAT.

Xiuqing Hu received the B.S. degree in atmospheric science from Nanjing University, Nanjing, China, in 1996 and the M.S. degree in cartography and geographical information system from Beijing Normal University, Beijing, China in 2004. He has been a part-time student of Ph.D. in quantitative remote sensing science in the Institute of Remote Sensing Application, Chinese Academy of Sciences, Beijing, China, since 2006.

From 1996 to 2004, he was a Research Assistant in the National Satellite Meteorological Center, China Meteorological Administration (NSMC/CMA). He was an Associate Professor and the Chief of CAL/VAL Branch of the Satellite Meteorological Institute of NSMC/CMA in 2004. He has been a Professor of engineering since 2010 and has been the Instrument Scientist of Medium Resolution Spectral Imager onboard Chinese FengYun-3 since 2006. Currently, he is a Visiting Scientist in NOAA/NESDIS/STAR, College Park, MD, as a Remote Sensing Senior Scientist. His research interests include calibration and validation for optical and infrared sensors, the retrieval algorithm of aerosol/dust and water vapor, and the climate data record from environment satellite.

Professor Hu is a Member of WMO Sand and Dust Storm Warning Advisory and Assessment System Regional Steering Group and a member of Global Space-based Inter-Calibration System Research Working Group.

Dohyeong Kim received the B.S. and M.S. degrees in earth science from Seoul National University, Seoul, Korea, in 1996 and 1998, respectively, and the Ph.D. degree in atmospheric science from the School of Earth and Environmental Sciences, Seoul National University, in 2003.

Currently, he is a Senior Researcher at the National Meteorological Satellite Center, Korea Meteorological Administration, concentrating on the development of Geo-KOMPSAT-2A (COMS follow-on) and calibration of COMS instrument.

Currently, Dr. Kim is a Member of WMO Expert Team on Satellite Systems and Co-Chair of the Research Working Group of the Global Space-based Inter-Calibration System Research Working Group.

Marianne Koenig received the M.S degree in meteorology from the University of Cologne, Cologne, Germany, in 1979 and the Ph.D. doctorate in meteorology from the same university, based on her work on derived radiation budget parameters from Meteosat observations.

Since 1995, she has been a Meteorological Scientist at EUMETSAT, Darmstadt, Germany, leading the algorithm development group focusing on meteorological products from the EUMETSAT geostationary satellites. She is a Member of the Global Space-based Inter-Calibration System Research Working Group.